Parameterizing Total Storm Conduction Currents Derived in a Global Model

Christina Kalb[1,*], Wiebke Deierling[1], Andreas Baumgaertner[2], Douglas Mach[3], Chuntao Liu[4] and Michael Peterson[5]

1. National Center for Atmospheric Research, Boulder, Colorado, USA
2. Department of Engineering, Aerospace Sciences, University of Colorado, Boulder, Colorado, USA
3. USRA, Huntsville, Alabama, USA
4. Texas A&M – Corpus Christi, Corpus, Christi, Texas, USA
5. University of Utah, Salt Lake City, Utah, USA

ABSTRACT: Electrified clouds are thought to play a major role in the global electric circuit. These clouds produce currents from the top of thunderstorms which help maintain the potential difference between earth's surface and the upper atmosphere. Previously, currents for different types of electrified clouds were estimated from overflights of the NASA ER-2 aircraft and compared with radar derived dynamical and microphysical properties (Deierling et al., this conference). In this study, high resolution model output from the Community Earth System Model (CESM) is compared with reanalysis data to determine the skill of CESM at representing these microphysical and dynamical properties of storms. Then, these storm properties are used to infer global distributions of conduction currents over different temporal scales and compared with data derived from the lightning imaging sensor (LIS) and precipitation radar (PR) measurements onboard the Tropical Rainfall Measuring Mission (TRMM) satellite.

INTRODUCTION

An electric field exists between earth's surface and the ionosphere, with a quasi-static potential of about 240 kV. It is thought that electrified clouds play an important role in maintaining this potential difference. These clouds produce an upward so-called Wilson current from the top of the cloud to the ionosphere which is thought to be the primary source for supplying current to the global electric circuit (Bering et al. 1998). However, not all clouds contribute equally and the exact current contribution from different types of clouds is not entirely known at this time.

Although several theories for cloud electrification exist, the non-inductive charging mechanism is thought to play a major role in thunderstorm electrification. (MacGorman and Rust 1998). In this mechanism, riming hydrometeors collide with ice crystals in the presence of supercooled liquid water resulting in opposite charge on the respective ice hydrometeors. Through gravitational sorting, the heavier rimed hydrometers reside mostly in the lower portion of the cloud and the ice crystals are transported to

* Contact information: Christina Kalb, National Center for Atmospheric Research, 3080 Center Green Drive Boulder, Colorado 80301-2252, United States, Email: kalb@ucar.edu

the upper parts of the cloud, creating net negative and positive charge regions inside the cloud. The magnitude of charge transfer depends on temperature, liquid water content, size of the ice crystals and impact velocity (e.g. Saunders and Peck 1998; Takahashi and Miyawaki 2002).

Consistent with the non-inductive charging mechanism, multiple observational studies, including studies based on radar observations, have shown a correlation between updraft speeds, mixed phase microphysics (between 0^{o}C and -40^{o}C) and the associated lightning. For example, Deierling et al. (2008) examined the relationship between precipitation ice mass fluxes for temperatures colder than -5^{o}C and lightning frequency for storms over Northern Colorado/Kansas and Northern Alabama. They found a good correlation between precipitation and non-precipitation ice mass as well as their fluxes and total lightning activity. Based on Tropical Rainfall Measuring Mission (TRMM) Precipitation Radar (PR) and Lightning Imaging Sensor (LIS) data, Petersen et al. (2005) found that radar derived ice water path above -10^{o}C was highly correlated to lightning flash density for data spanning three years in the tropics and subtropics. Liu et al. (2012) used thirteen years of TRMM PR data and examined multiple radar based variables in relation to LIS lightning data. They found high correlations between lightning flash rates and radar reflectivities greater than 30, 35, and 40 dBZ between 0^{o}C and -40^{o}C. They also noted that these relationships varied between oceanic and continental storms.

Several studies have also examined the relationship between storm updrafts and lightning characteristics. Wiens et al. (2005) examined one supercell in northern Colorado, and found that total flash rates correlated well with the volume of updraft speeds greater than 10 ms^{-1}. Deierling and Petersen (2008) examined storms over Northern Colorado, Kansas, and Alabama. They found the best correlations between updraft volume for temperatures colder than -5 and -10^{o}C with vertical velocities greater than 5 and 10 m s^{-1} and total lightning flash rates. Furthermore, recent studies also suggest that these storm microphysical and dynamical properties may represent storm conduction currents (Mach et al. 2010; Davydenko et al. 2009).

A comprehensive model of the global electric circuit which can be incorporated into available community models does not exist at this time. As a first step toward parameterizing the role of electrified clouds in the global electric circuit, this study uses high resolution model output from the Community Earth System Model (CESM) and compares it with reanalysis data from the NCAR Climate Four Dimensional Data Assimilation (CFDDA) system and precipitation feature data from the Tropical Rainfall Measuring Mission (TRMM). The goal is to determine whether CESM has skill at representing these microphysical and dynamical properties of storms and the associated storm currents.

DATA AND METHODS

Models

1) CESM

CESM, developed primarily at the National Center for Atmospheric Research (NCAR), is a fully-coupled, community, global climate model. The atmospheric component, CAM, includes all relevant dynamical, physical, and chemical processes of the troposphere and stratosphere on horizontal scales of 10 to 100km. Descriptions and evaluation of the model components are contained in the CESM4 special collection of the Journal of Climate.

Here, we employ two configurations of the model, a high-resolution, free-running simulation for June 2005 with the extended physics of CAM5, denoted S-highres hereafter, and a low-resolution simulation with CAM4 physics, nudged with GEOS-5 reanalysis for all of 2005, denoted S-lowres hereafter. Both simulations use model version CESM1.1.1, and were initialized from observations in 2000.

Cloud physics in CAM as well as the convective schemes employed are particularly relevant for this study. Neale et al. (2010) provides a general overview of these schemes. In brief, both CAM4 and CAM5, use the Zhang-McFarlane scheme for deep convection. However, the scheme is modified by adding convective momentum transport according to Richter and Rasch (2008) and a modified dilute plume calculation following Raymond and Blyth (1986, 1992). For shallow convection, CAM5 uses the scheme from Park and Bretherton (2009), whereas CAM4 used the Hack (1994) scheme. Note that the schemes do not include formation mechanisms of cloud hydrometeor and precipitation inside convective updrafts. However, microphysics is included in the model based loosely on the approach from Morrison et al. (2005), which is a 2 moment microphysics scheme that includes cloud droplets and cloud ice.

2) CFDDA Reanalysis

The CESM data was compared with the NCAR CFDDA system (Hahmann et al. 2010; Rife et et al. (2010). Reanalysis data offers the benefits of a regular grid and high time resolution allowing the diurnal cycle to be examined. CFDDA is a global reanalysis based on the PSU/NCAR Mesoscale Model (MM5) which uses NCAR's Real Time Four Dimensional Data Assimilation system (Liu et al. 2008). Data assimilation is achieved using a Newtonian relaxation technique (Stauffer et al. 1991; Stauffer and Seaman 1994; Seaman et al. 1995) which nudges the model to observations, for small scale features, and toward the National Centers for Environmental Prediction-Department of Energy Atmospheric Model Intercomparison Project (AMIP-II) Reanalysis (Kanamitsu et al. 2002) for upper air and larger scale features.

Observations are ingested continuously and include standard surface and upper air rawindsondes and satellite derived temperature, humidity, and winds. Convection is represented in the model using the Kain-Fritsch version 2 (Kain 2004) cumulus parameterization and the microphysics scheme developed by Reisner et al. (2008), which includes four hydrometer species, cloud water, cloud ice, rain, and snow. Both, CESM and CFDDA were examined visually and then downsampled to a 1 degree grid, as well as smoothed using a 4 degree by 4 degree two dimensional low pass finite impulse response filter for a grid point to grid point comparison with global current distributions derived from TRMM observations.

Current Data

Global total storm current distributions were computed from a precipitation and cloud feature database from Liu et al. (2010), which is based on TRMM observations. This database contains counts of thunderstorms and electrified shower clouds in 1 degree grid boxes between 35 South and 35 North latitude. Mach et al. (2010) derived mean current estimates from 850 aircraft overflights for thunderstorms and electrified shower clouds as 1.7 and 0.41A over oceans and 1.0 A and 0.13 A over land. These values were multiplied by the storm counts to produce a total current for each grid box.

Methods

Several variables were selected from the model and reanalysis data that represent the updraft and mixed phased characteristics expected to affect cloud electrification. From CESM, this included in cloud

ice water content and convective mass flux. To isolate the region where thunderstorm electrification occurs, in cloud ice water content was integrated starting at 500 hPa pressure upwards. Convective mass flux data were integrated above 850hPa. In addition total precipitation rate was investigated from both CESM and CFDDA.

The model and reanalysis variables were divided based on geographic location of land, ocean, and coast, as several studies have shown regional differences in lightning distributions and flash rates (Boccippio et al. 2000; Mach et al. 2007; Mach et al. 2010; Liu et al. 2012). For each grid box, land was defined as having greater than 90 percent land mass, ocean was less than 10 percent land mass, and coast having between 10 and 90 percent land. The model data were averaged over a month to represent the northern hemisphere summer (June 2005) and across the entire 2005 year. In addition, the model data were compared directly to the TRMM current data.

RESULTS

CESM and CFDDA Total Precipitation

Figure 1 shows average total precipitation in June 2005 for CESM S-highres and CFDDA. In general, the CFDDA rain rates are larger than CESM, and the field is smoother. This may be partially due to the lower resolution of CFDDA. However, Monaghan et al. (2010) examined the CFDDA rainfall and found that CFDDA typically produced higher rainfall estimates than either the Climate Prediction Center Morphing Technique (CMORPH) or the Global Precipitation Climatology Project 1 Degree Daily Combination product estimates. The values though, were not outside the range of uncertainty. Also, CESM shows much smaller precipitation rates over the tropical western Pacific Ocean and the local maxima off the western coast of Central America and Papua New Guinea are weaker and shifted westward when compared to CFDDA. Zhang and Mu (2005) examined this behavior in detail and determined that the cause of this low precipitation is the result small convective available potential energy values (CAPE) in this region. In the Zhang-MacFarlane scheme, convection is proportional to CAPE (Zhang and MacFarlane 1995).

Figure 2 shows scatterplots of TRMM derived global storm current distributions (Figure 3, upper panel) versus CESM and CFDDA total rain over oceans, land, and coasts respectively for June 2005. The blue line in Figure 2 represents a linear regression fit to the data. Data from coastal regions show the highest correlation between TRMM distributions and those for CESM and CFDDA respectively with correlation coefficients of 0.766 and 0.763. Data from oceanic regions is also similar, but both CESM and CFDDA output contain several outliers with rain rates above 0.8 mm h^{-1} and currents between 0.15 and 0.2 A. The land data shows the most variance in CESM as there is a region of scatter with precipitation rates greater than 0.45 mm h^{-1} and currents greater than 0.05 A.

Several studies have examined the relationship between rainfall and lightning activity (Williams et al., 1992; Petersen and Rutledge, 1998; Soriano et al., 2001). These studies showed a positive correlation between convective rainfall and lightning activity, but found that exact relationship was strongly regime dependent. This is because precipitation in the tropics can often be dominated by warm rain processes whereas heavy precipitation in the midlatitudes and over land generally requires vigorous mixed phase microphysics. It is thought that mixed phase microphysics contribute significantly to thunderstorm electrification. Our results here reflect such regime dependence also for total rainfall activity and Wilson

currents, as both models show oceanic regions to have the least increase in rain rates versus current (regression coefficient of 0.21 mm h^{-1} A^{-1} and 0.19 mm h^{-1} A^{-1}), whereas land and coastal regions have regression coefficients that range between 0.25 and 0.29 mm h^{-1} A^{-1}. A longer duration dataset comparison of TRMM precipitation data and CESM as well as CFDDA output will be performed in the future to investigate how representative these results are.

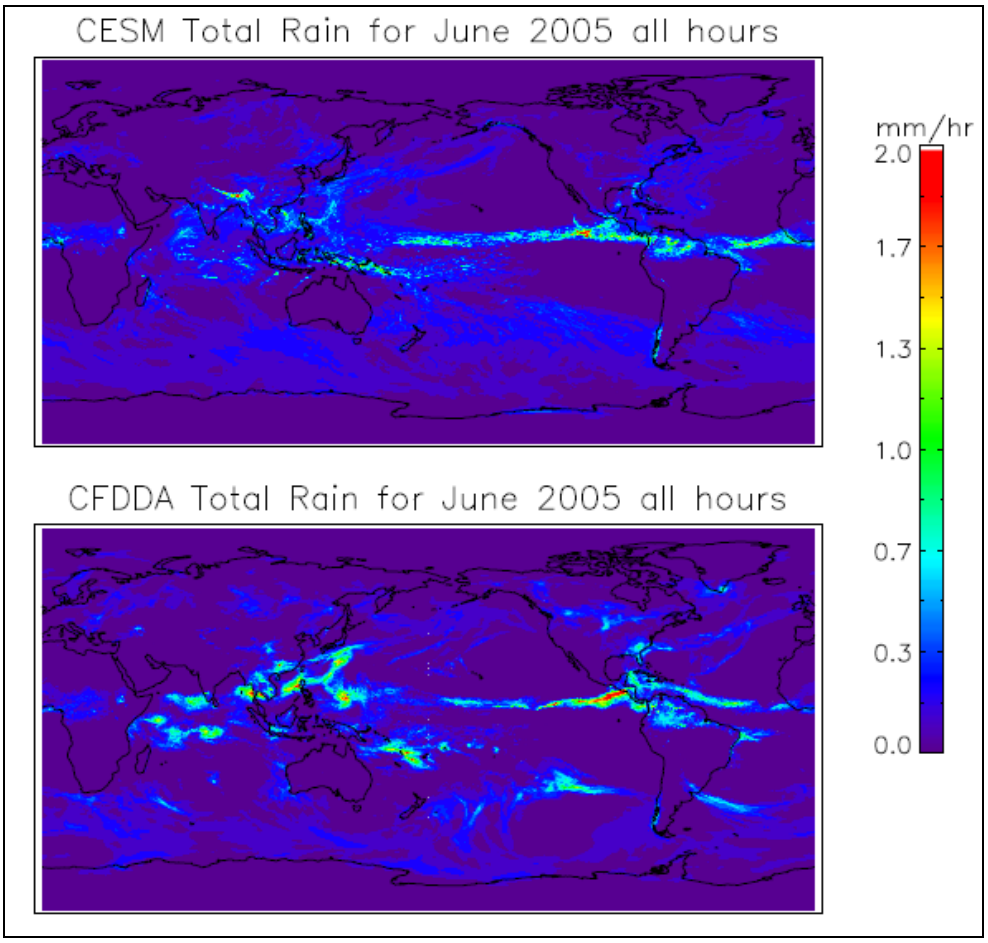

Figure 1. Total precipitation rate averaged over June 2005 for CESM S-highres (top) and CFDDA (bottom).

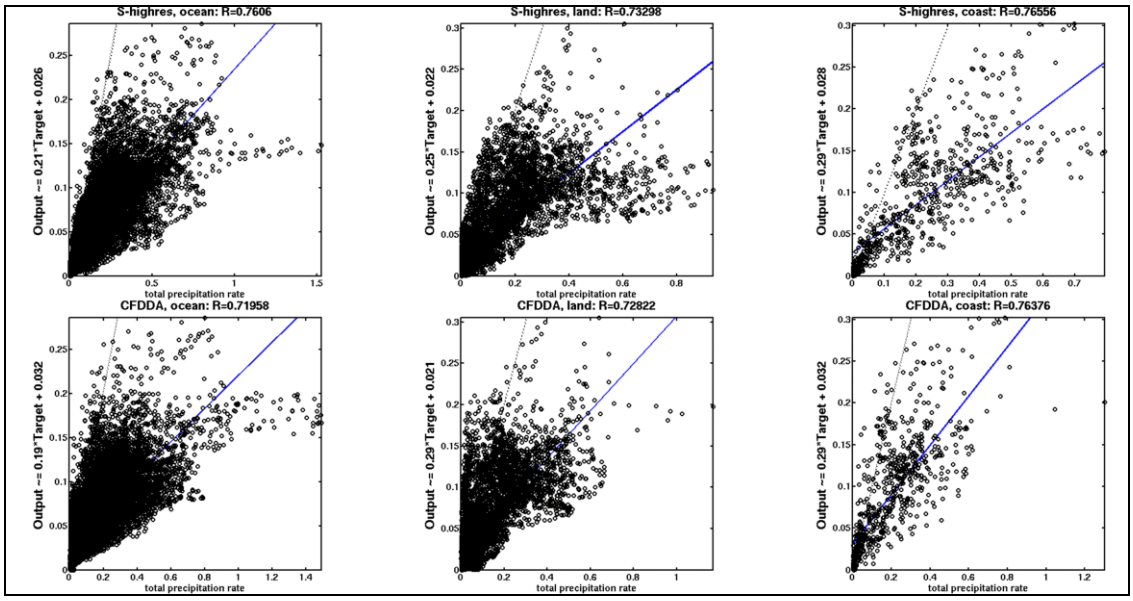

Figure 2. Scatterplots for the TRMM currents versus CESM (top) and CFDDA (bottom) total precipitation rate for oceans (left), land (middle) and coasts (right). The blue line is a regression fit to the data.

CESM convective mass flux and ice water path

CESM S-highres convective updraft mass flux and in cloud ice water path are shown in Figure 3 along with the TRMM current data. Both variables capture the main features shown in the current data, including the intertropical convergence zone (ITCZ) in the Pacific and Atlantic Oceans and local maxima over Africa, Costa Rica and Panama. However, local maxima in currents over the Philippines and Malaysia exhibited by the global current TRMM distribution are under-represented in convective mass flux and ice water path. Also, both variables show a local maximum off the eastern coast of India that differs from the TRMM derived global current distribution.

Comparing CESM and the TRMM derived total current sources on a gridpoint by gridpoint basis, Figure 4 shows scatterplots of convective mass flux for 2005 using S-lowres against total storm currents. The coastal and oceanic regions exhibit good correlations with correlation coefficients of r=0.808 and 0.749 respectively. Land areas are associated with a poorer correlation of r=0.677. In addition, the CESM land data shows a region of scatter below the regression line. The line may be skewed by the few data points with convective mass fluxes above 5 kg m^{-2} s^{-2} and currents between 0.08 and 0.14 A. The regression lines are similar for land and oceans with slopes of 22 kg m^{-2} s^{-2} A^{-1}, whereas coastal regions show a steeper slope of 31 kg m^{-2} s^{-2} A^{-1}.

In comparison to convective mass flux, ice water path shows more scatter for the oceans and land, reflected by the lower correlation coefficients of r=0.683 and r=0.441 respectively. Similar to convective mass flux, the coastal regions have the best correlation coefficient (r=0.806) with land being the poorest. The land data also have the flattest regression line with a slope of 0.012 kg m^{-2} A^{-1} compared to 0.014 kg m^{-2} A^{-1} for oceans and 0.024 kg m^{-2} A^{-1} for coasts. Petersen et al. (2005) suggested that the relationship between ice water path and lightning flash density was independent of convective regime. CESM does

show different relationships for oceanic, land and in particular different coastal regimes. Liu et al. (2012) also showed a regime dependence between land, oceans, and coastal regions, although they show the largest slope for the land and coastal regimes. In contrast, for the four weeks of data CESM shows the largest slope for only the coastal regions.

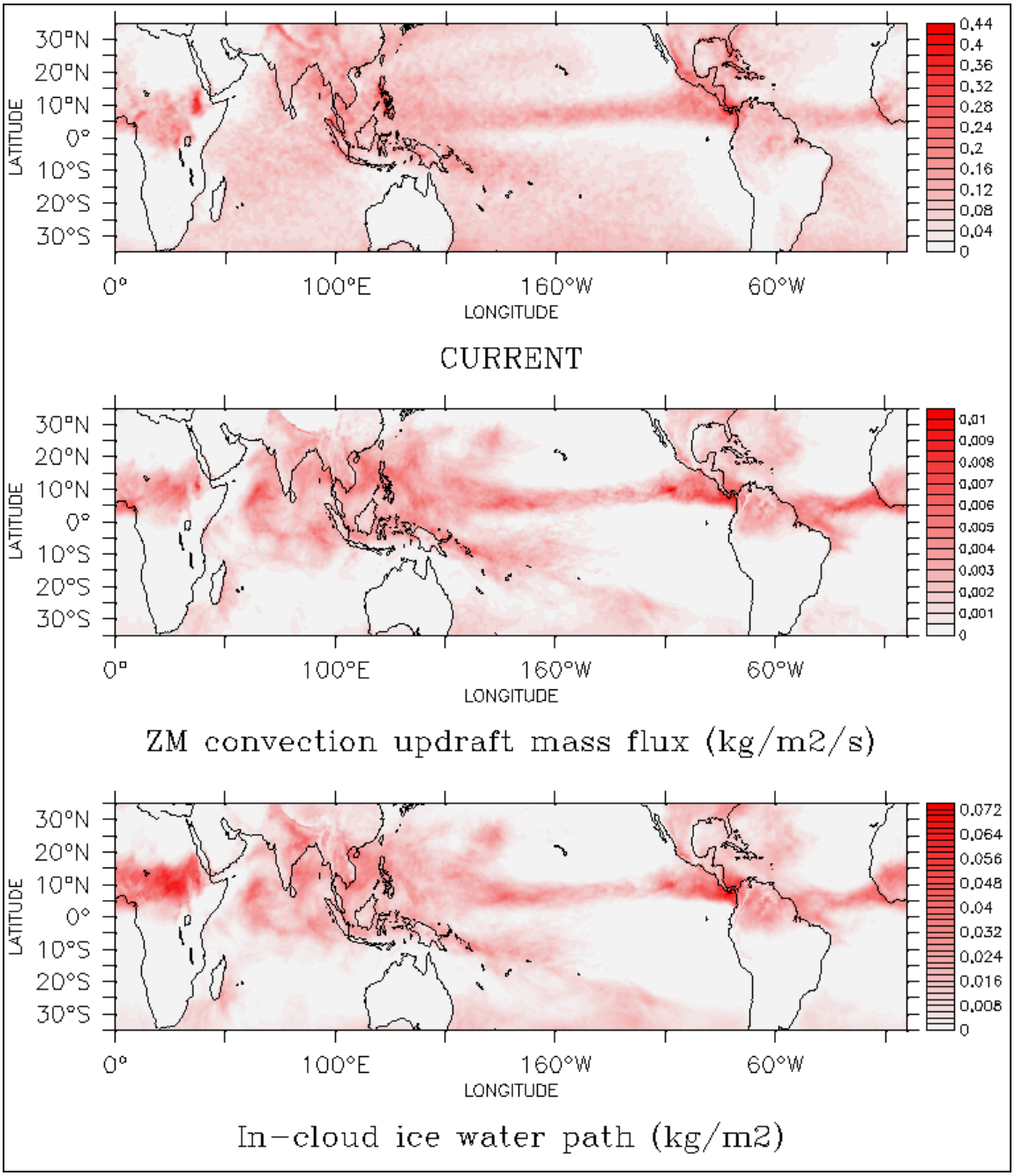

Figure 3. TRMM Current data in A (top), CESM S-highres convective mass flux (middle), and CESM S-highres ice water path (bottom) for June 2005.

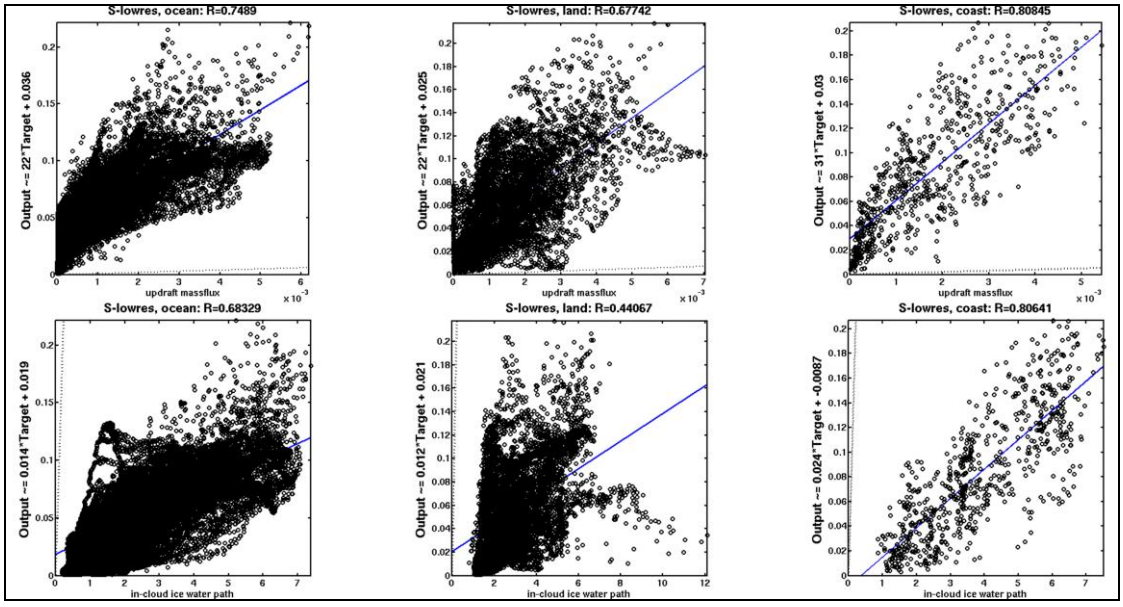

Figure 4. Scatterplots the TRMM currents versus CESM S-lowres convective mass flux (top) and ice water path (bottom) for oceans (left), land (middle) and coasts (right). The blue line is a regression fit to the data.

Carnegie Curves

The Carnegie Curve (Figure 5) represents the diurnal variation of the fair weather electric field as measured aboard the ship Carnegie between 1915 and 1929. Several studies have noted that the Carnegie curve matches the diurnal variation of lightning activity and thunderdays (Whipple 1929; Whipple and Scrase 1936), with a slight mismatch in amplitude (Mach et al. 2011). Here we derive a Carnegie curve using the CESM S-highres convective mass flux averaged globally and over the month of June. Figure 6 shows the Carnegie curve derived from CESM convective mass flux S-lowers (left) and S-highres (right). Comparing S-lowres to Figure 5, the diurnal minimum occurs slightly earlier at 0100 UTC than the Carnegie curve at 0300 UTC. The maximum of the CESM derived curve also occurs early at 1500 UTC rather than at 1900 UTC as seen in the observed Carnegie curve. In addition, the amplitude of the CESM based curve is smaller than observed amplitude peaking at 12% deviation from the mean whereas the observed Carnegie curve shows deviations of 15 % from the mean.

The S-highres curve has a slightly better representation of the minimum, occurring at 0400 UTC compared to Carnegie curve at 0300 UTC, but the maximum is still early at 1500 UTC. In addition, the amplitude is much less than both the S-lowres and Carnegie curve amplitude at a 6% variation compared to 12% and 15% respectively. Figure 7 shows the globally averaged convective mass flux plotted over time for the month of June. It can be seen that the diurnal cycle of the Carnegie curve is captured by the convective mass flux variable. It can also be seen that the amplitude varies across different days with a minimum daily variation of 0.001 kg m^{-2} s^{-1} and a maximum daily variation of approximately 0.00025 kg m^{-2} s^{-1}.

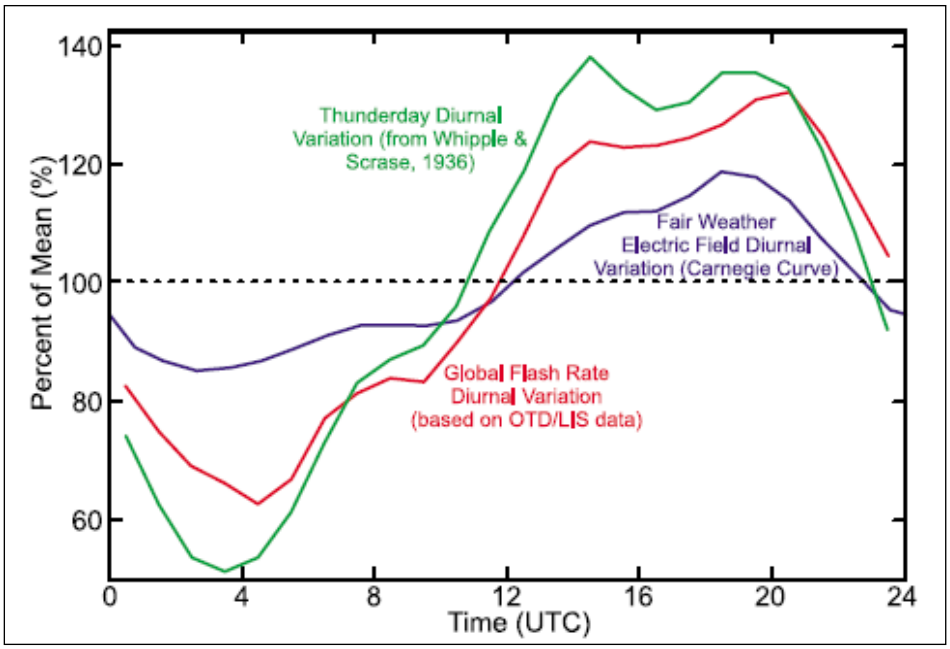

Figure 5. The Carnegie curve (purple) compared with the diurnal thunderday variation (green), and the diurnal global flash rate variation (red), from Mach et al. 2011.

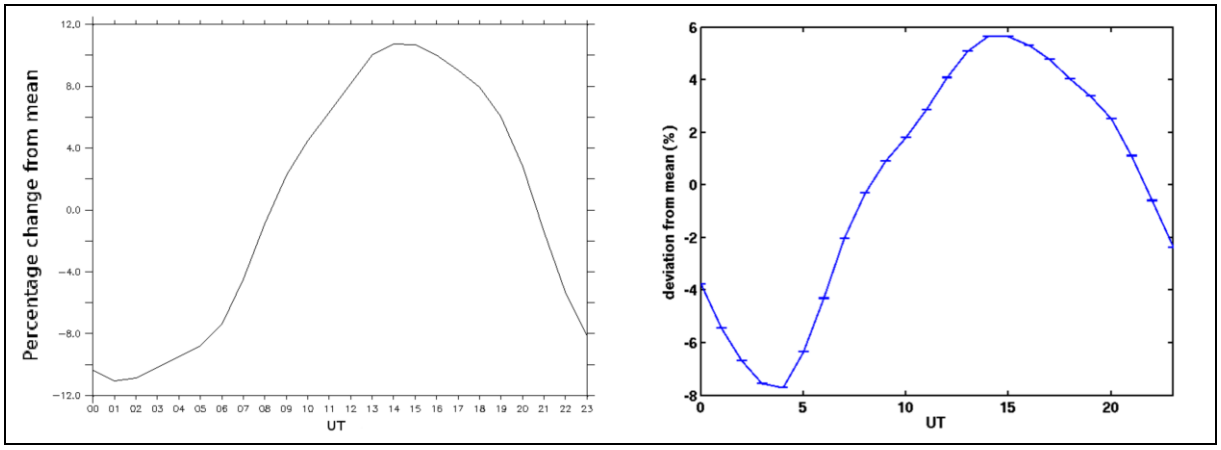

Figure 6. Two Carnegie curves for CESM convective mass flux using S-lowres for all of 2005 (left) and S-highres for June 2005 (right) averaged globally. Note that the 0 on this axis corresponds to 100 in the previous image.

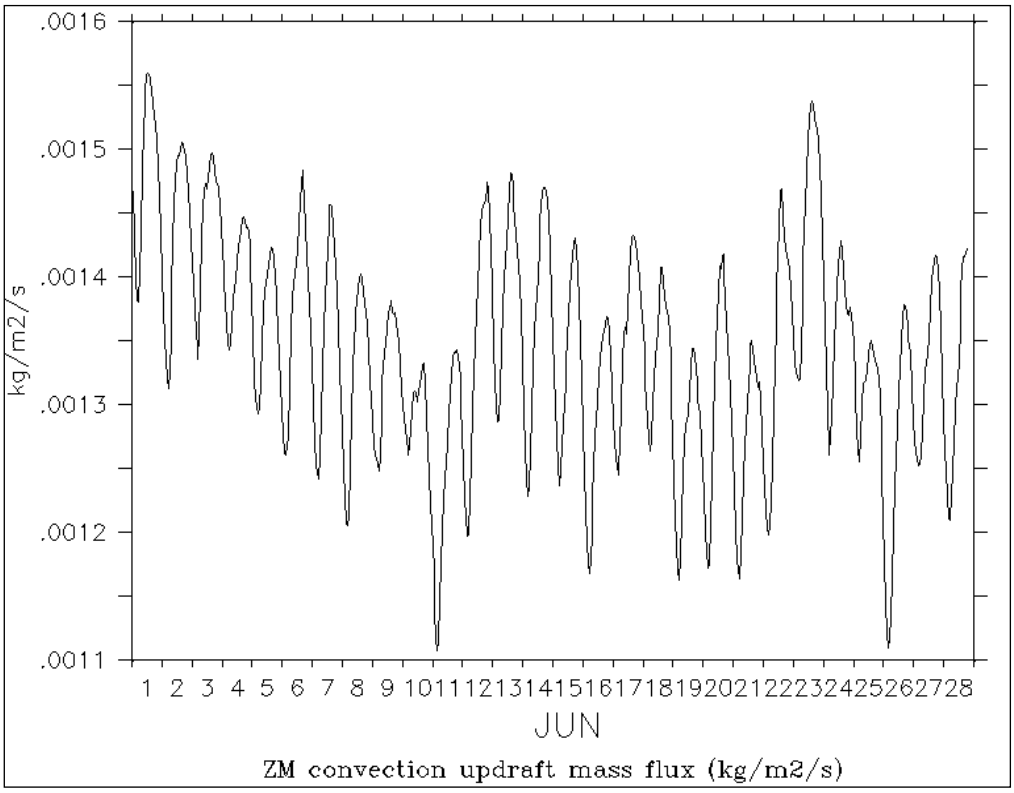

Figure 7. Diurnal variation in convective mass flux averaged globally for June 2005.

CONCLUSIONS

Using high resolution model output from CESM, global reanalysis data from CFDDA, and precipitation feature data from TRMM, this study examines the model representation of Wilson currents derived from microphysical and dynamical properties of storms previously shown to correlate well with cloud electrification and lightning. The goal is to determine the model skill at predicting Wilson currents based on these variables. This work is a first step toward parameterizing the role of electrified clouds in the global electric circuit for use in a comprehensive global model such as WACCM that is based on a global climate model to describe the lower atmosphere.

We compared several model parameters to global TRMM derived Wilson current distributions. Total precipitation averaged for June 2005 from CESM generally shows a lower rain rate than what is seen in CFDDA. For the most part, the patterns of precipitation agree well in both datasets, except over the western Pacific Ocean. When the data is separated into different convective regimes of land, ocean, and coast, positive correlations are seen between precipitation rate and conduction currents. However, oceanic regions have the least increase in rain rates versus current in agreement with previous studies.

Both convective mass flux and ice water path averaged over June 2005 agree well with the geographical patterns seen in the TRMM current estimates. Yearly, convective mass flux shows a positive correlation to the current data that is fairly consistent between land, oceans, and coastal regions. In comparison, ice water path shows considerably more scatter and the coastal regions show the steepest regression coefficient.

Examining the diurnal cycle, the Carnegie curves derived from the CESM convective mass flux S-

lowres and S-highres are fairly similar to the ship derived Carnegie curve when averaged globally for June 2005. However, the maximum occurs 4 hours earlier and the amplitudes are less at 12% and 6% variations about the mean compared with the Carnegie Curve 15%. Overall, convective mass flux shows the best skill at representing the current data from TRMM.

These results suggest that CESM output parameters may have skill at representing cloud microphysical variables for the tropics and subtropics (35 North to 35 degrees South). However, it is unclear how the results would be affected by including data from the midlatitudes. In addition, model data spanning more than a single year would also be needed to test the robustness of these results.

ACKNOWLEDGMENTS

This work was partly funded by National Science Foundation Frontiers in Earth System Dynamics grant 1135446. The National Center for Atmospheric Research is sponsored by the National Science Foundation.

REFERENCES

Bering III, E. A., A. A. Few, and J. R. Benbrook, 1998: The Global Electric Circuit, *Phys. Today*, **51**, 24-32.

Boccippio, D. J., S. J. Goodman, and S. Heckman, 2000: Regional differences in tropical lightning distributions, *J. Appl. Meteorol.*, **39**, 2231-2248.

CCSM4 Special Collection, 2011-2014, Journal of Climage, http://journals.ametsoc.org/page/CCSM4/CESM1.

Davydenko, S. S., T. C. Marshall, and M. Stolzenburg, 2009: Modeling the electric structures of two thunderstorms and their contributions to the global electric circuit. *Atmos. Res.*, **91**, 165-177.

Deierling, W., W. A. Petersen, J. Latham, S. Ellis, and H. J. Christian, 2008: The relationship between lightning activity and ice fluxes in thunderstorms. *J. Geophys. Res.*, **113**, D15210, doi:10.1029/2007JD009700.

Deierling, W., and W. A. Petersen, 2008: Total lightning activity as an indicator of updraft characteristics. *J. Geophys. Res.*, **113**, D16210, doi:10.1029/2007JD009598.

Hack, J. J., 1994: Parameterization of moist convection in the National Center for Atmospheric Research Community Climate Model (CCM2). *J. Geophys. Res.*, **99**, 5551-5568.

Hahmann, A. N., D. Rostkier-Edelstein, T. T. Warner, F. Vandenberghe, Y. Liu, R. Babarsky, and S. P. Swerdlin, 2010: A reanalysis system for the generation of mesoscale climatographies. *J. Appl. Meteor. Climatol., 49*, 954-972.

Jayarantne, E. R., C. P. R. Saunders, and J. Hallett, 1983: Laboratory studies of the charging of soft hail during ice crystal interactions. *Quar. J. Roy. Meteor. Soc.*, **101**, 227-234.

Kain, J. S., 2004: The Kain-Fritsch convective parameterization: An update. *J. Appl. Meteor.*, **43**, 170-181.

Kanamitsu, M., W. Ebisuzaki, J. Woolen, S. K. Yang, J. J. Hnilo, M. Fiorino, and G. L. Potter, 2002: NCEP-DOE AMIP-II Reanalysis (R-2). *Bull. Amer. Meteor. Soc.*, **83**, 1631-1643.

Keith, W. D., and C. P. R. Saunders, 1990: Further laboratory studies of the charging of graupel during ice crystal interactions. *Atmos. Res.*, **25**, 445-464.

Liu, C., E. Zipser, D. Cecil, S. W. Nesbitt, and S. Sherwood, 2008: A cloud and precipitation feature database from 9 years of TRMM data. *J. Appl. Meteor. Climatol.*, **47**, 2712-2728.

Liu, C., E. R. Williams, E. Zipser, and G. Burns, 2010: Diurnal variations of global thunderstorms and electrified shower clouds and their contribution to the global electrical circuit. *J. Atmos. Sci.*, **67**, 309-323.

Liu, C., D. J. Cecil, E. J. Zipser, K. Kronfeld, and R. Robertson, 2012: Relationships between lightning flash rates and radar reflectivity vertical structures in thunderstorms over the tropics and subtropics. *J. Geophys. Res.*, **117**, D062121, doi:10.1029/2011JD017123.

Liu, Y., and Coauthors, 2008: The operational mesogamma-scale analysis and forecast system of the U. S. Army Test and Evaluation Command, Part I: Overview of the modeling system, the forecast products, and how the products are used. *J. Appl. Meteor. Climatol.*, **47**, 1077-1092.

MacGorman, D. R., and W. D. Rust, 1998: The Electrical Nature of Storms. Oxford University Press, 422 pp.

Mach, D. M., H. J. Christian, R. J. Blakeslee, D. J. Boccippio, S. J. Goodman, and W. L. Boeck, 2007: Performance assessment of the optical transient detector and lightning imaging sensor, *J. Geophys. Res.*, **112**, D09210, doi:10.1029/2006JD007787.

Mach, D. M., R. J. Blakeslee, M. G. Bateman, and J. C. Bailey, 2010: Comparisons of total currents based on storm location, polarity, and flash rates derived from high-altitude aircraft overflights. *J. Geophys. Res.*, **115**, D03201, doi:10.1029/2009JD012240.

Mach, D. M., R. J. Blakeslee, and M. G. Bateman, 2011: Global electric circuit implications of combined aircraft storm electric current measurements and satellite-based diurnal lightning statistics. *J. Geophys. Res.*, **116**, D05201. doi:10.1029/2010JD014462.

Monaghan, A. J., D. L. Rife, J. O. Pinto, and C. A. Davis, 2010: Global precipitation extremes associated with diurnally varying low-level jets. *J. Climate*, **23**, 5065-5084.

Morrison, H., J. A. Curry, and V. I. Khvorostyanov, 2005: A new double-moment microphysics parameterization for application in cloud and climate models. part i: Description, *J. Atmos. Sci.*, **62**, 1665–1677.

Neale, R. B., et al., 2010, Description of the NCAR Community Atmosphere Model (CAM 5.0), NCAR Technical Note, http://www.cesm.ucar.edu/models/cesm1.0/cam/docs/description/cam5_desc.pdf.

Park, S. and C. S. Bretherton, 2009: The University of Washing shallow convection and moist turbulence schemes and their impact on climate simulations with the Community Atmosphere Model. *J. Climate*, **22**, 3449-2469.

Petersen, W. A., and S. A. Rutledge, 1998: On the relationship between cloud-to-ground lightning and convective rainfall. *J. Geophys. Res.*, **103**, 14,025-14,040.

Petersen, W. A., H. J. Christian, and S. A. Rutledge, 2005: TRMM observations of the global relationship between ice water content and lightning. Geophys. Res. Lett., 32, L14819, doi:10.1029/2005GL023236.

Raymond, D. J., and A. M. Blyth, 1986: A stochastic mixing model for non-precipitating cumulus clouds. *J. Atmos. Sci.*, **43**, 2708-2718.

Raymond, D. J., and A. M. Blyth, 1992: Extension of the stochastic mixing model to cumulonimbus clouds. *J. Atmos. Sci.*, **49**, 1968–1983.

Reisner, J. M., R. M. Rasmussen, and R. T. Bruintjes, 1998: Explicit forecasting of supercooled liquid water in winter storms using the MM5 forecast model. *Quart. J. Roy. Meteor. Soc.*, **124**, 1071-1107.

Richter, Jadwiga H., and Philip J. Rasch. 2008: Effects of convective momentum transport on the atmospheric circulation in the Community Atmosphere Model version 3, *Journal of Climate*, **21.7**, 1487-499.

Rife, D. L., J. O. Pinto, A. J. Monaghan, and C. L. Davis, 2010: Global distribution and characteristics of diurnally varying low-level jets. *Journal of Climate*, **23**, 5041-5064.

Saunders, C.P.R., and S.L. Peck, 1998: Laboratory studies of the influence of the rime accretion rate on charge transfer during crystal/graupel collisions. *J. Geophys. Res.*, **103**, 13949-13956.

Seaman, N. L., D. R. Stauffer, and A. M. Lario-Gibbs, 1995: A multiscale four-dimensional data assimilation system applied in the San Joaquin Valley during SARMAP. Part I: Modeling design and basic performance characteristics. *J. Appl. Meteor.*, **34**, 1739-1761.

Soriano, L. R., F. DePablo, and E. G. Diez, 2001: Relationship between convective precipitation and cloud-to-ground lightning in the Iberian Peninsula. *Mon. Wea. Rev.*, **129**, 2998-3003.

Stauffer, D. R., and N. L. Seaman, 1994: Multiscale four-dimensional data assimilation. *J. Appl. Meteor.*, **33**, 416-434.

Stauffer, D. R., N. L. Seaman, and F. S. Binkowski, 1991: Use of four-dimensional data assimilation in a limited-area mesoscale model. Part II: Effects of data assimilation withing the planetary boundary layer. *Mon. Wea. Rev.*, **119**, 734-754.

Takahashi, T., and K. Miyawaki, 2002: Reexamination of riming electrification in a wind tunnel. *J. Atmos. Sci.*, **59**, 1018-1025.

Whipple, F. J., 1929: On the association of the diurnal variation of electric potential gradient in fine weather with the distribution of thunderstorms over the globe. *Quart. J. Roy. Meteor. Soc.*, **55**, 1-17.

Whipple, F. J., and F. J. Scrase, 1936: Point-discharge in the electric field of the earth, *Geophys Mem. VII*, **68**, 1-20.

Wiens, K. C., S. A. Rutledge, and S. A. Tessendorf, 2005: The 29 June 2000 Supercell observed during STEPS. Part II: Lightning and charge structure. *J. Atmos. Sci.*, **62(12)**, 4151-4177.

Williams, E. R., S. A. Rutledge, S. C. Geotis, N. Renno, E. Rasmussen, and T. Rickenbach, 1992: A radar and electrical study of tropical hot towers. *J. Atmos. Sci.*, **49**, 1386-1395.

Zhang, G. J., and N. A. McFarlane, 1995: Sensitivity of climate simulations to the parameterization of cumulus convection in the Canadian Climate Centre general circulation model. *Atmosphere-Ocean,* **33.3**, 407-46.

Zhang, G. J., and M. Mu, 2005: Effects of modifications to the Zhang-MacFarlane convection parameterization on the simulation of the tropical precipitation in the National Center for Atmospheric Research Community Climate Model, version 3. *J. Geophys. Res.*, **110**, D09109, doi:10.1029/2004JD005617.